X-RAY OUTFLOWS AND SUPER-EDDINGTON ACCRETION IN THE ULTRALUMINOUS X-RAY SOURCE HOLMBERG IX X-1

D. J. Walton[1], J. M. Miller[2], F. A. Harrison[1], A. C. Fabian[3], T. P. Roberts[4], M. J. Middleton[5], and R. C. Reis[2]

[1] Space Radiation Laboratory, California Institute of Technology, Pasadena, CA 91125, USA
[2] Department of Astronomy, University of Michigan, 500 Church Street, Ann Arbor, MI 48109, USA
[3] Institute of Astronomy, University of Cambridge, Madingley Road, Cambridge, CB3 0HA, UK
[4] Department of Physics, Durham University, South Road, Durham DH1 3LE, UK
[5] Astronomical Institute Anton Pannekoek, University of Amsterdam, Postbus 94249, NL-1090 GE Amsterdam, The Netherlands

ABSTRACT

Studies of X-ray continuum emission and flux variability have not conclusively revealed the nature of ultraluminous X-ray sources (ULXs) at the high-luminosity end of the distribution (those with $L_X \geqslant 10^{40}$ erg s^{-1}). These are of particular interest because the luminosity requires either super-Eddington accretion onto a black hole of mass $\sim 10 \, M_\odot$ or more standard accretion onto an intermediate-mass black hole. Super-Eddington accretion models predict strong outflowing winds, making atomic absorption lines a key diagnostic of the nature of extreme ULXs. To search for such features, we have undertaken a long, 500 ks observing campaign on Holmberg IX X-1 with *Suzaku*. This is the most sensitive data set in the iron K bandpass for a bright, isolated ULX to date, yet we find no statistically significant atomic features in either emission or absorption; any undetected narrow features must have equivalent widths less than 15–20 eV at 99% confidence. These limits are far below the $\gtrsim 150$ eV lines expected if observed trends between mass inflow and outflow rates extend into the super-Eddington regime and in fact rule out the line strengths observed from disk winds in a variety of sub-Eddington black holes. We therefore cannot be viewing the central regions of Holmberg IX X-1 through any substantial column of material, ruling out models of spherical super-Eddington accretion. If Holmberg IX X-1 is a super-Eddington source, any associated outflow must have an anisotropic geometry. Finally, the lack of iron emission suggests that the stellar companion cannot be launching a strong wind and that Holmberg IX X-1 must primarily accrete via Roche-lobe overflow.

Key words: black hole physics – X-rays: binaries – X-rays: individual (Holmberg IX X-1)

Online-only material: color figures

1. INTRODUCTION

Ultraluminous X-ray sources (ULXs) are off-nuclear point sources found in nearby galaxies that require extraordinary accretion-power. The nature of the most luminous sources within this class—those with $L_X \geqslant 10^{40}$ erg s^{-1} (e.g., Farrell et al. 2009; Walton et al. 2011b; Sutton et al. 2012; Jonker et al. 2012)—is particularly interesting. These sources may be standard stellar-remnant black holes ($M_{BH} \sim 10 \, M_\odot$) accreting at super-Eddington rates (Poutanen et al. 2007; Finke & Böttcher 2007), or intermediate-mass black holes ($10^2 \, M_\odot \lesssim M_{BH} \lesssim 10^5 \, M_\odot$) accreting at sub-Eddington rates (Miller et al. 2004; Strohmayer & Mushotzky 2009). Indeed, the high-luminosity end of the ULX distribution may include both extremes, or even a continuum in between (Zampieri & Roberts 2009). ULXs with $L_X \geqslant 10^{40}$ erg s^{-1} represent a regime in which our knowledge of black hole accretion can be extended and tested. For recent reviews focusing on ULXs see Roberts (2007) and Feng & Soria (2011).

A robust prediction for accretion at high rates (near Eddington or above) is that strong outflows or winds should be launched from the accretion disk (Shakura & Sunyaev 1973; Poutanen et al. 2007; Ohsuga & Mineshige 2011; Dotan & Shaviv 2011; Vinokurov et al. 2013). Indeed, Galactic stellar mass black holes (StMBHs) at moderately high accretion rates (states dominated by thermal disk emission) frequently display evidence for such disk winds (Miller et al. 2006; Neilsen & Lee 2009; King et al. 2012) with outflow velocities $v_{out} \lesssim 10,000$ km s^{-1}. When these outflows cover our line of sight to the central source, absorption features are imprinted onto the intrinsic X-ray continuum, the most prominent of which are typically the Kα transitions of highly ionized iron (Fe xxv and/or xxvi). As expected, the strength of the outflows observed appears to increase with the inferred accretion rate in both StMBHs (Ponti et al. 2012) *and* in active galactic nuclei (AGNs; King et al. 2013). For sub-Eddington StMBHs, outflows are seen predominantly in high inclination sources, so the outflow geometry is inferred to be roughly equatorial. Numerical simulations of winds from thin (sub-Eddington) disks further support such an outflow geometry (Proga & Kallman 2004).

The majority of ULXs have luminosities of a few $\times 10^{39}$ erg s^{-1}, and likely represent a high luminosity extension of the disk-dominated thermal states observed in Galactic StMBHs (Kajava & Poutanen 2009; Middleton et al. 2013). Outflow geometries in these cases are likely to still be largely equatorial. However, a common prediction of super-Eddington accretion and the subsequent outflows is that as the accretion rate increases, the solid angle subtended by the outflow should also increase (Abramowicz 2005; King 2009; Dotan & Shaviv 2011). At the high Eddington rates required to explain the $L_X \geqslant 10^{40}$ erg s^{-1} ULXs (assuming $M_{BH} \sim 10 \, M_\odot$), one might expect that atomic iron features associated with a strong, large solid angle outflow would be a common feature of the X-ray spectra.

Walton et al. (2012) describe initial searches for iron features in ULX spectra, using archival *XMM-Newton* data for two bright ($L_X \sim 10^{40}$ erg s^{-1}) sources, Holmberg IX X-1 and NGC 1313 X-1. No statistically significant features were found in either source and the limits obtained required any lines to be relatively weak in comparison to simple scaling of the sub-Eddington

features observed from other accreting black holes up to the super-Eddington regime. In order to enhance the sensitivity to atomic iron features, we undertook deep observations of the luminous source Holmberg IX X-1 with *Suzaku*. In this Letter we present the results from our search for X-ray spectral features in the iron-K energy range with this new data set.

2. DATA REDUCTION

Holmberg IX X-1 was observed for a total exposure of ∼500 ks during 2012 by the *Suzaku* observatory (Mitsuda et al. 2007). To extract science products, we reprocessed the unfiltered event files for each of the XIS CCDs (XIS0, 1, 3; Koyama et al. 2007) and editing modes ($3 \times 3, 5 \times 5$) operational using the latest HEASOFT software package (version 6.13), as recommended in the Suzaku Data Reduction Guide.[6] Cleaned event files were generated by re-running the *Suzaku* pipeline with the latest calibration, as well as the associated screening criteria files. For each of the observation segments, source products were extracted with XSELECT from circular regions ∼200″ in radius and the background was extracted from adjacent regions free of any contaminating sources, with care taken to avoid the calibration sources in the corners. Instrumental responses were generated for each individual spectrum using the XISRESP script with a medium resolution. The spectra and response files for the front-illuminated (FI) detectors (XIS0, 3) were combined using the FTOOL ADDASCASPEC. Finally, we grouped the spectra to have a minimum signal-to-noise ratio of 5 per energy bin with the SPECGROUP task (part of the *XMM-Newton* SAS), to allow the use of χ^2 minimization during spectral fitting.

2.1. HXD PIN

Due to the level of systematic uncertainty in the PIN background model ($\gtrsim 25\%$ of the "source" flux given the weak detection of the Holmberg IX field; see, e.g., discussion in Walton et al. 2013) and the variable nature of the contaminating M 81 nucleus (Markoff et al. 2008; Miller et al. 2010), it is not possible to constrain the high energy ($E > 10$ keV) properties of Holmberg IX X-1 with the collimating PIN detector. The imaging capabilities of the recently launched *NuSTAR* observatory (Harrison et al. 2013) are required. Therefore, we do not consider the PIN data here and stress that any interpretation based on these data should be regarded with extreme skepticism.

3. SPECTRAL ANALYSIS

Throughout this work, spectral modeling is performed with XSPEC v12.8.0 (Arnaud 1996) and absorption by intervening neutral material is treated with TBNEW (Wilms et al. 2000) using the appropriate solar abundances. We include two absorption components, one fixed at the Galactic column ($N_{H;Gal} = 5.54 \times 10^{20}$ atom cm^{-2}; Kalberla et al. 2005) and another with variable column at the redshift of Holmberg IX ($z = 0.000153$). During modeling, we only consider data from the FI detectors in the 1–10 keV energy range, owing to a calibration mismatch between XIS0 and XIS3 below ∼1 keV. For the same reasons, we only consider data from the back-illuminated (BI) XIS1 detector over the 2.5–9.0 keV energy range. We also exclude the 1.6–2.5 keV energy range from the FI data owing to remaining calibration uncertainties associated with the instrumental silicon K and gold M edges, and the 7.3–7.6 keV energy range from the BI data owing to a residual background
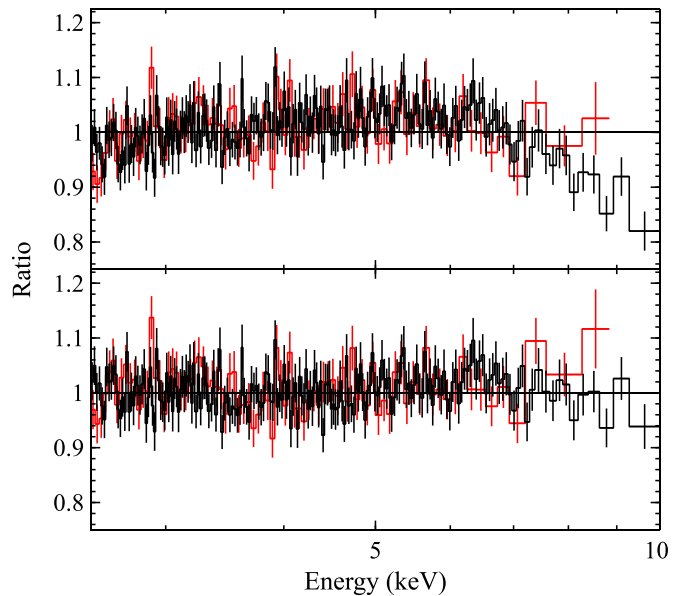
Figure 1. 2.5–10.0 keV data/model ratios of the full Holmberg IX X-1 *Suzaku* data set to a simple powerlaw ($\Gamma = 1.72 \pm 0.01$; top panel) and a powerlaw with a high energy cut-off ($\Gamma = 1.27 \pm 0.07$, $E_{cut} = 10^{+2}_{-1}$ keV; bottom panel). The latter provides a far superior fit to the data, indicating a curved continuum is favored.

(A color version of this figure is available in the online journal.)

feature. The data from the FI and BI detectors are modeled simultaneously, with all parameters tied between the spectra, and we attempt to account for any further cross-calibration uncertainties above 2.5 keV by allowing a variable multiplicative cross-normalization constant to vary between them. This value is always found to be within ∼10% of unity.

3.1. Continuum Modeling

We begin with a brief assessment of the form of the continuum, focusing first on the 2.5–10.0 keV energy range. Specifically, we wish to determine whether a simple powerlaw-like continuum is sufficient, or whether there is evidence for curvature similar to other high quality ULX data sets (Stobbart et al. 2006; Gladstone et al. 2009; Walton et al. 2011a). Similar to previous works, we compare the results obtained with a simple powerlaw continuum, with and without a high energy exponential cut-off. We indeed find that allowing a cut-off offers a significant improvement ($\Delta\chi^2 = 135$, one additional free parameter; see Figure 1), i.e., the 2.5–10.0 keV spectrum does show curvature.

Considering the 1–10 keV bandpass, we utilize a common parameterization of the continuum for ULXs, modeling the data with cool, optically thick Comptonization (Stobbart et al. 2006; Gladstone et al. 2009; Middleton et al. 2011; Walton et al. 2011a). We note that this parameterization is largely empirical and should not be ascribed too much physical significance. The nature of the continuum emission will be addressed in more detail in future work (D. J. Walton et al., in preparation) utilizing the necessary *NuSTAR* data. Here, we use the COMPTT code (Titarchuk 1994), which provides an excellent fit ($\chi^2_\nu = 1730/1694$). As we do not consider the data below 1 keV, we are not sensitive to the presence of any additional low-temperature (∼0.2 keV) thermal component similar to those seen previously in bright, unabsorbed ULXs (Miller et al. 2004), so we fix the seed photon temperature to 0.1 keV. The continuum parameters

Table 1
Continuum Parameters Obtained for Holmberg IX X-1

Component	Parameter	Value
TBNEW (Galactic)	N_H (cm^{-2})	5.54×10^{20} (fixed)
TBNEW (intrinsic)	N_H (cm^{-2})	$(8 \pm 2) \times 10^{20}$
	z	0.000153 (fixed)
COMPTT	T_{seed} (keV)	0.1 (fixed)
	T_e (keV)	2.6 ± 0.1
	τ	$7.1^{+0.3}_{-0.2}$
χ^2_ν		1730/1694

obtained are summarized in Table 1, and are broadly similar to those obtained with previous observations (Gladstone et al. 2009; Vierdayanti et al. 2010; Walton et al. 2012).

3.2. Narrow Iron K Features

Walton et al. (2012) describe constraints on atomic iron K features for ULXs, focusing on the archival *XMM-Newton* data available for Holmberg IX X-1, revisited here with *Suzaku*, and NGC 1313 X-1. In order to search for atomic features in this new dedicated data set, we follow the same approach adopted in that work, varying a narrow ($\sigma = 10$ eV) Gaussian across the 5–9 keV energy range, to include the rest frame energies of the iron K transitions and also generously allow for the possibility of blueshifted features, in steps of 0.04 keV. For each energy step, we record the $\Delta\chi^2$ improvement resulting from the inclusion of the Gaussian line, as well as the best fit equivalent width (EW) and its 90% and 99% confidence limits.[7] The latter quantities are obtained with the EQWIDTH command in XSPEC, generating 10,000 parameter sets based on the best fit model and the covariance matrix, which includes information on the model parameter uncertainties, and extracting the confidence limits from the distribution of EWs obtained.

The results obtained are shown in Figure 2. The top panel shows the $\Delta\chi^2$ improvement, multiplied by the sign of the best fit normalization to differentiate between emission and absorption and the limits on EW obtained are shown in the bottom panel. For clarity, we highlight the energies of the Kα transitions of neutral, helium-like, and hydrogen-like iron, as well as EW = ± 30 eV, representative of the strongest absorption features observed in GRS 1915+105 (Neilsen & Lee 2009). In addition, we also show the limits we obtained previously with *XMM-Newton*. As in our previous analysis, we find no statistically significant line detections, so we again focus on the limits that can be placed instead. Any narrow atomic features in the *Suzaku* data in the immediate Fe K band (6–7 keV) must have EWs of less than ∼15–20 eV (99% confidence); previously we were only able to constrain such features to EW $\lesssim$ 30 eV. On average, the allowed EW range at a given energy is a factor of ∼1.5 smaller with our new data set than obtained previously (Walton et al. 2012).

4. DISCUSSION

Using our long 500 ks *Suzaku* observation of Holmberg IX X-1, we have undertaken the deepest study in the Fe K region of a bright, isolated ULX to date to search for iron absorption/ emission features similar to those frequently observed in other

---

[7] We again note that we are computing confidence limits on line strength, which are not formally the same as the upper limits on the strength of lines that should be detected at a given confidence level (Kashyap et al. 2010), but are simpler to calculate and provide more conservative estimates for the maximum strength of any lines intrinsically present.
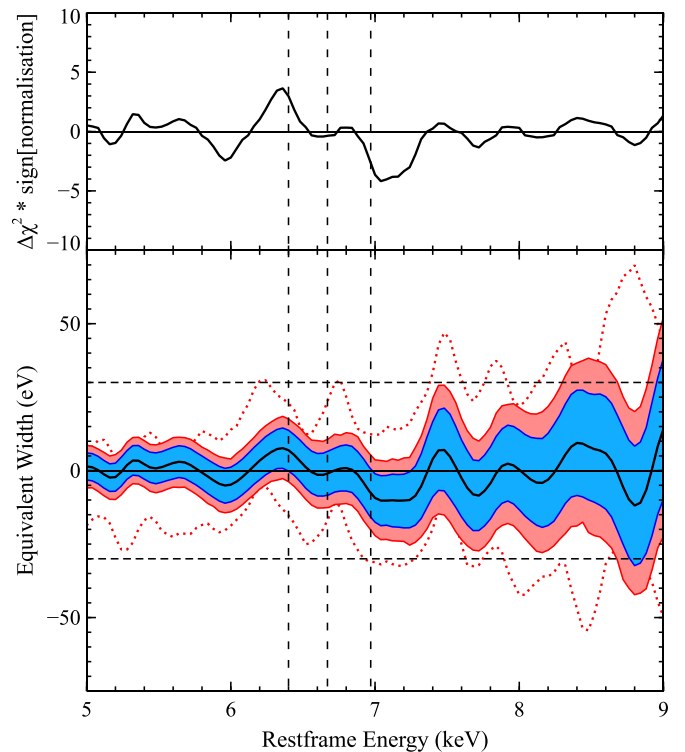

Figure 2. Top panel: the $\Delta\chi^2$ improvement provided by a narrow Gaussian line, as a function of (rest frame) line energy for the full *Suzaku* Holmberg IX X-1 data set. Positive (negative) values of $\Delta\chi^2$ indicate the improvement is obtained with an emission (absorption) line. We find no compelling evidence for any narrow iron K features. Bottom panel: 90% (blue) and 99% (red) confidence contours for the equivalent width of a narrow line, indicating the line strengths of any narrow features intrinsically present could have and still remain undetected. The rest frame transitions of neutral, helium-like, and hydrogen-like iron (6.4, 6.67, and 6.97 keV) are shown with vertical dashed lines, and we also plot dashed horizontal lines representing EW = ± 30 eV. Finally, we also show the 99% EW limits obtained from archival *XMM-Newton* data in Walton et al. (2012) for direct comparison (red dotted lines).

(A color version of this figure is available in the online journal.)

accreting black holes. Iron is ideally suited to identifying the presence of atomic processes, as it is both difficult to fully ionize and cosmically abundant. Despite the high sensitivity of the observations, we do not detect any discrete atomic iron features. The limits on any persistent narrow features (either in emission or absorption) as yet undetected are now EW $\lesssim$ 15–20 eV (99% confidence) over the immediate Fe K energy range.

As shown in Figure 3, these limits are now extremely restrictive when considered in the context of the lines observed from other sources. Remarkably, in terms of absorption, the constraints are such that any iron features present in Holmberg IX X-1 must be *weaker* than the absorption lines observed in numerous sub-Eddington Galactic StMBHs (Miller et al. 2006; Neilsen & Lee 2009; King et al. 2012) and AGN (Tombesi et al. 2010; Gofford et al. 2013). Meanwhile, any neutral iron emission from Holmberg IX X-1 must be weaker than that observed in the vast majority of Galactic high-mass X-ray binaries (HMXBs), which ubiquitously display such emission features (Torrejón et al. 2010), and there cannot be any substantial emission from helium- or hydrogen-like iron either. At the energies of these transitions, the 99% limits on emission lines are EW < 15, 11, and 4 eV respectively.

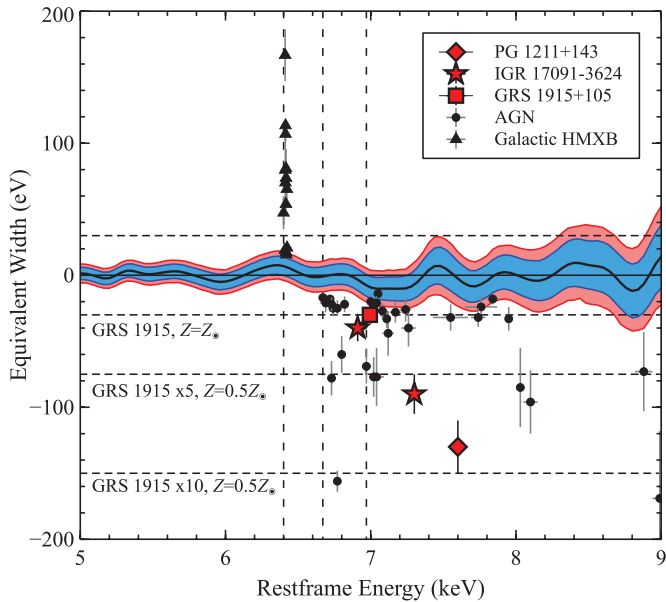It is clear from the lack of absorption features that we cannot be viewing the central hard X-ray emitting regions of

Figure 3. Line limits obtained for Holmberg IX X-1 placed in the broader context of the absorption features detected in both AGN (Tombesi et al. 2010; Gofford et al. 2013) and selected Galactic StMBHs (Neilsen & Lee 2009; King et al. 2012), and the emission lines detected in Galactic HMXBs (Torrejón et al. 2010). Some notable sources have been highlighted. For further comparison, we also show the GRS 1915+105 absorption (assumed solar metallicity) scaled up by factors of 5 and 10, accounting for the metallicity of Holmberg IX ($\sim$0.5 $Z_\odot$; Makarova et al. 2002). These may be conservative scalings for the expected EW, as the mass outflow rate should increase faster than linearly with Eddington ratio.

(A color version of this figure is available in the online journal.)

Holmberg IX X-1 through any substantial column of partially ionized material. We can therefore exclude the presence of any massive, spherical outflow in Holmberg IX X-1, as discussed in King & Pounds (2003), and wind-dominated spectral models (Vierdayanti et al. 2010) are also ruled out. If Holmberg IX X-1 truly is a StMBH accreting substantially in excess of the Eddington limit, we must be viewing it through a line of sight that is not covered by the massive outflow launched in such an accretion regime. The most natural conclusion is that, in this scenario, we would have to be viewing the source close to face-on (see also Roberts et al. 2011), with the wind still retaining some kind of roughly equatorial geometry, broadly similar to that inferred for sub-Eddington disk winds (Ponti et al. 2012), although presumably with a much larger scale-height for both the disk and the outflow (Poutanen et al. 2007). Furthermore, our results require that any equatorial outflow must be launched further out than the central hard X-ray emitting region, despite this presumably being the most irradiated region of the accretion flow. If this is the case, observation of atomic iron emission from such a massive outflow might be expected instead. The expected line profile might well be more complex than a simple narrow Gaussian; however, we stress that there are no clear residual features that would readily be interpreted as re-emission from a strong wind, which may prove problematic for any extreme super-Eddington scenario. This will be addressed in more detail in future work.

The lack of narrow iron emission lines has strong implications for the broader nature of the accretion onto Holmberg IX X-1, regardless of the black hole mass. In many respects, ULXs are widely expected to be analogues to black hole HMXBs. However, Galactic HMXBs ubiquitously display neutral iron emission lines (Torrejón et al. 2010), owing to illumination of the

stellar winds in which they are embedded and from which they may primarily accrete. Since there is no iron emission observed, either neutral or highly ionized, we infer that either the stellar wind is weak (or even absent) or the accretion geometry is such that this material is not illuminated by the hard X-rays emitted from the central regions.

Returning to the possible scenario in which ULXs are powered by a large scale height, optically thick super-Eddington accretion flow, the inner regions of such accretion flows are expected to have a roughly conical geometry with the hard X-rays being produced in the hotter, central regions. If this funnel covers a large enough solid angle, it may be able to shield the majority of the stellar wind from the hard X-rays, which would be scattered and collimated preferentially out of the equatorial plane. Given the expected large-scale extent of the stellar wind, the optically thick regions of the accretion flow would have to cover an extremely large solid angle in order to prevent substantial iron line emission. However, the observed luminosity of the He II λ4686 emission line, presumed to be associated with the cool outer disk, appears to require that the X-ray luminosity cannot be highly anisotropic via photon counting arguments (Moon et al. 2011). Optical/UV photometry is also indicative of X-ray reprocessing in the outer disk (Grisé et al. 2011), so it is not clear that this offers a self-consistent scenario.

Alternatively, if the scale height of the accretion flow is not sufficient to provide substantial shielding, the lack of iron emission would therefore tell us that there is no strong stellar wind. Indeed, for a spherically symmetric reprocessing geometry, which works well for Galactic HMXBs (Torrejón et al. 2010), and the metallicity of Holmberg IX ($\sim$0.5 $Z_\odot$; Makarova et al. 2002), the specific emission line limits obtained for neutral and hydrogen-like iron correspond to reprocessing columns of $N_H \lesssim 10$ and 3×10^{22} atom cm^{-2}, respectively (see Walton et al. 2012). For comparison, the HMXBs analyzed by Torrejón et al. (2010), which have companion masses $M_* \gtrsim 10\ M_\odot$, typically display columns of $N_H \gtrsim 10^{23}$ atom cm^{-2}. In turn, these observational constraints mean that any stellar wind present most likely cannot provide the mass accretion rate of $\dot{M} \gtrsim 1.5 \times 10^{-6}\ M_\odot$ yr^{-1} required to power the observed X-ray luminosity from Holmberg IX X-1. Instead, Holmberg IX X-1 most likely accretes via Roche-lobe overflow, as suggested by Grisé et al. (2011), the accretion mechanism more typically associated with low-mass X-ray binaries (LMXBs). However, Galactic LMXBs are generally transient sources, spending the majority of the time in quiescence, occasionally undergoing accretion events resulting in bright $\sim$month-to-year long X-ray outbursts. In contrast, Holmberg IX X-1 appears to be a much more persistent source, requiring a sufficiently close binary system such that Roche-lobe overflow/mass transfer remains roughly continuous. Grisé et al. (2011) found a lower limit to the mass of the stellar companion of $M_* \gtrsim 10\ M_\odot$. We suggest that the absent/weak stellar wind implies that the companion cannot be substantially more massive than this lower limit, given that more massive stars generally launch stronger winds.

Finally, in addition to improving the narrow line limits, we also confirm the presence of curvature in the $\sim$3–10 keV energy range, as previously indicated by *XMM-Newton* (Gladstone et al. 2009). We defer a detailed consideration of the continuum to future work, which will focus on broadband spectral analysis utilizing the required *NuSTAR* data, although we do comment here that the 3–10 keV spectrum does not appear consistent with the power-law-like emission expected from a standard sub-Eddington corona.

5. CONCLUSIONS

Our long *Suzaku* program on Holmberg IX X-1 has provided the most sensitive data set in the Fe K region obtained for any luminous, isolated ULX to date. Despite the high sensitivity of these data, we find no statistically significant narrow atomic features in either emission or absorption across the 5–9 keV energy range. Furthermore, the data are of sufficient quality to limit any undetected features to have EW of $\lesssim$ 15–20 eV across the immediate Fe K bandpass at 99% confidence, i.e., weaker than the features associated with sub-Eddington outflows in a number of other black holes. Therefore, we cannot be viewing the central hard X-ray emitting regions of Holmberg IX X-1 through any substantial column of material. Models of spherical super-Eddington accretion can be rejected, as can wind-dominated spectral models. If Holmberg IX X-1 is accreting at highly super-Eddington rates, our viewing angle must be close to face on, such that the associated outflow is directed away from our line-of-sight. Finally, the lack of iron emission implies that the stellar companion is unlikely to be launching a strong wind, and therefore the black hole must primarily accrete via Roche-lobe overflow.

REFERENCES

Abramowicz, M. A. 2005, in Growing Black Holes: Accretion in a Cosmological Context, ed. A. Merloni, S. Nayakshin, & R. A. Sunyaev (Berlin: Springer), 257
Arnaud, K. A. 1996, in ASP Conf. Ser. 101, Astronomical Data Analysis Software and Systems V, ed. G. H. Jacoby & J. Barnes (San Francisco, CA: ASP), 17
Dotan, C., & Shaviv, N. J. 2011, MNRAS, 413, 1623
Farrell, S. A., Webb, N. A., Barret, D., Godet, O., & Rodrigues, J. M. 2009, Natur, 460, 73
Feng, H., & Soria, R. 2011, NewAR, 55, 166
Finke, J. D., & Böttcher, M. 2007, ApJ, 667, 395
Gladstone, J. C., Roberts, T. P., & Done, C. 2009, MNRAS, 397, 1836
Gofford, J., Reeves, J. N., Tombesi, F., et al. 2013, MNRAS, 430, 60
Grisé, F., Kaaret, P., Pakull, M. W., & Motch, C. 2011, ApJ, 734, 23
Harrison, F. A., Craig, W. W., Christensen, F. E., et al. 2013, ApJ, 770, 103

Jonker, P. G., Heida, M., Torres, M. A. P., et al. 2012, ApJ, 758, 28
Kajava, J. J. E., & Poutanen, J. 2009, MNRAS, 398, 1450
Kalberla, P. M. W., Burton, W. B., Hartmann, D., et al. 2005, A&A, 440, 775
Kashyap, V. L., van Dyk, D. A., Connors, A., et al. 2010, ApJ, 719, 900
King, A. L., Miller, J. M., Raymond, J., et al. 2012, ApJL, 746, L20
King, A. L., Miller, J. M., Raymond, J., et al. 2013, ApJ, 762, 103
King, A. R. 2009, MNRAS, 393, L41
King, A. R., & Pounds, K. A. 2003, MNRAS, 345, 657
Koyama, K., Tsunemi, H., Dotani, T., et al. 2007, PASJ, 59, 23
Makarova, L. N., Grebel, E. K., Karachentsev, I. D., et al. 2002, A&A, 396, 473
Markoff, S., Nowak, M., Young, A., et al. 2008, ApJ, 681, 905
Middleton, M. J., Miller-Jones, J. C. A., Markoff, S., et al. 2013, Natur, 493, 187
Middleton, M. J., Sutton, A. D., & Roberts, T. P. 2011, MNRAS, 417, 464
Miller, J. M., Nowak, M., Markoff, S., Rupen, M. P., & Maitra, D. 2010, ApJ, 720, 1033
Miller, J. M., Raymond, J., Fabian, A. C., et al. 2004, ApJ, 601, 450
Miller, J. M., Raymond, J., Fabian, A., et al. 2006, Natur, 441, 953
Mitsuda, K., Bautz, M., Inoue, H., et al. 2007, PASJ, 59, 1
Moon, D.-S., Harrison, F. A., Cenko, S. B., & Shariff, J. A. 2011, ApJL, 731, L32
Neilsen, J., & Lee, J. C. 2009, Natur, 458, 481
Ohsuga, K., & Mineshige, S. 2011, ApJ, 736, 2
Ponti, G., Fender, R. P., Begelman, M. C., et al. 2012, MNRAS, 422, L11
Poutanen, J., Lipunova, G., Fabrika, S., Butkevich, A. G., & Abolmasov, P. 2007, MNRAS, 377, 1187
Proga, D., & Kallman, T. R. 2004, ApJ, 616, 688
Roberts, T. P. 2007, Ap&SS, 311, 203
Roberts, T. P., Gladstone, J. C., Goulding, A. D., et al. 2011, AN, 332, 398
Shakura, N. I., & Sunyaev, R. A. 1973, A&A, 24, 337
Stobbart, A.-M., Roberts, T. P., & Wilms, J. 2006, MNRAS, 368, 397
Strohmayer, T. E., & Mushotzky, R. F. 2009, ApJ, 703, 1386
Sutton, A. D., Roberts, T. P., Walton, D. J., Gladstone, J. C., & Scott, A. E. 2012, MNRAS, 423, 1154
Titarchuk, L. 1994, ApJ, 434, 570
Tombesi, F., Cappi, M., Reeves, J. N., et al. 2010, A&A, 521, A57
Torrejón, J. M., Schulz, N. S., Nowak, M. A., & Kallman, T. R. 2010, ApJ, 715, 947
Vierdayanti, K., Done, C., Roberts, T. P., & Mineshige, S. 2010, MNRAS, 403, 1206
Vinokurov, A., Fabrika, S., & Atapin, K. 2013, AstBu, 68, 139
Walton, D. J., Gladstone, J. C., Roberts, T. P., et al. 2011a, MNRAS, 414, 1011
Walton, D. J., Miller, J. M., Reis, R. C., & Fabian, A. C. 2012, MNRAS, 426, 473
Walton, D. J., Nardini, E., Fabian, A. C., Gallo, L. C., & Reis, R. C. 2013, MNRAS, 428, 2901
Walton, D. J., Roberts, T. P., Mateos, S., & Heard, V. 2011b, MNRAS, 416, 1844
Wilms, J., Allen, A., & McCray, R. 2000, ApJ, 542, 914
Zampieri, L., & Roberts, T. P. 2009, MNRAS, 400, 677